# Theoretical Aspects of Electron Localizability

*Miroslav Kohout, Frank R. Wagner, Alexei I. Baranov, Carina Bergner, Viktor Bezugly, and Kati Wagner*

## Introduction

The chemical bonding in a molecule or solid can be analyzed from different viewpoints. Of great importance is the decision about what should be the basis of an analysis of the bonding situation.
On one hand, the particular components of the wavefunction of the system (respectively the corresponding density matrix) can serve as the basis for the desired bonding descriptors. Then, separate molecular orbitals or valence bonds can be examined and overlap integrals, occupation numbers and weights of structures computed. Such an approach is pictorially very appealing and serves as more or less solid background for the rationalization of chemical structures as well as in classrooms where the basics of quantum chemistry are taught. However, such objects as orbitals are just mathematical instruments to describe many- body wavefunctions, which in turn are mathematical objects serving as the basis for the description of density matrices.

On the other hand, functions created by the action of a suitable operator on the wavefunction and the combination of such functions can be analyzed. Following this viewpoint the Laplacian of electron density, different kinetic energy functions, gradient fields, etc. can be inspected and reasonable bonding descriptors searched for. This viewpoint can be extended to functionals based on integrals of density matrices over particular space regions. In this case the approach depends on the choice of the density matrix as well as the integration regions. For instance, the electron density (i.e., the diagonal part of the 1-matrix) integrated over regions bounded by the surface of zero-flux in the electron density gradient (so called basins or "atoms" in the QTAIM approach [1]) yields the electronic populations in the corresponding regions and thus, the charge of the "atomic" units. Similarly, the integrals of the 2-matrix over two chosen basins give access to the delocalization indexes [2]. Such a viewpoint can further be generalized to evaluate not just the integral for a single region, but a whole distribution of integrals over regions determined by a suitable space partitioning. The basic idea behind this approach is to examine the desired property (given density matrix integral) under the same conditions specified by a fixed amount of chosen (control) quantity.

## Electron Localizability

The expectation value of an operator is given as the integral of the action of the operator on the density matrix over the whole space. If the whole space is partitioned into non-overlapping mutually exclusive space filling regions, then this integration can be performed over each region separately and finally, the results can be summed up. In case of a single variable there are only integrals over each region, whereas for integrals dependent on two variables there are also terms in which each variable runs over different regions. Consequently, the total integral (expectation value) is given as a sum of two terms – the intra-region values and the inter-region values.

The regions could have any form. To get a local effect the regions must be "compact". We define the "compactness" by minimizing the sum of variances of the coordinates around the mean coordinate of each region. In other words, each region should be as "spherical" as possible.
To get regions of the same "quality" we require the integral of a chosen function (the control property) to yield the same fixed value $\omega$ for each region (termed a $\mu$-cell) of the partitioning. Such a partitioning procedure will be termed the $\omega$-restricted space partitioning [3].

Now, another function (the sampling property) can be integrated over the $\mu$-cells of the partitioning. For instance, the population in each $\mu$-cell can be determined. This procedure yields a discrete distribution of charges that can be analyzed. For a given sampling property the values of the integrals depend on the value of the $\omega$-restriction. However, if the restriction is small enough, then the values will scale with the restriction. The scaling can be removed to yield an $\omega$-restriction independent expression.

Let us adopt for the term localizability the view that it describes the tendency of a single electron to be separated from the other electrons. Thus, the motion of the single electron is correlated with the motion of the other ones [4]. High localizability means that the electrons try to avoid each other.

Such avoidance can be quantified by means of the charge sampled over μ-cells enclosing a fixed number of electron pairs (restricted populations approach). The resulting expression is called electron localizability indicator, abbreviated ELI-D (to emphasize the electron pair restriction). The values of ELI-D are proportional to the probability that the population (charge) in a μ-cell can be attributed to a single electron (with all other electrons outside the μ-cell). It shows to which extent the μ-cell is (spatially) occupied by a single electron. This approach can be realized at any level of theory as long as the electron density and electron pair density are accessible [5]. In Fig. 1 the real space representation of ELI-D for the $C_{60}$ molecule is presented. The high ELI-D values between the carbon atoms indicate that in those regions the same-spin electrons avoid each other.

For the density matrices given in the momentum space representation the whole procedure can be applied without any changes. The corresponding momentum space form of ELI-D describes to which extent a certain region of momenta can be attributed to a single electron [6]. Fig. 2 demonstrates the momentum space representation of ELI-D for the $C_{60}$ molecule. It can be seen that the same-spin electrons are localized in particular regions of momenta. In a general case the localizability value for a certain momentum region is generated from the 2-matrix data of the whole real space (Fourier transformation). Direct correspondence between the real space and momentum space regions of localizability can be achieved only in case of localized orbitals [6].

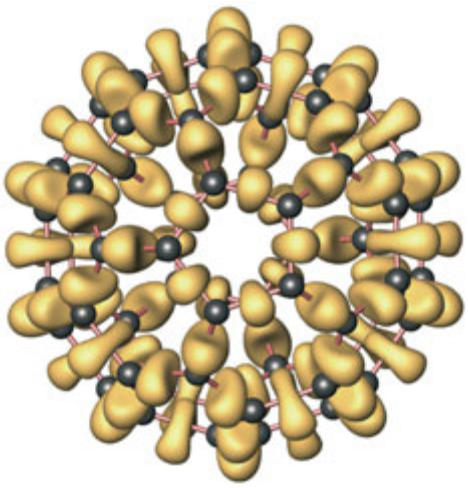

*Fig. 1: Position space representation of ELI-D for the $C_{60}$ molecule.*

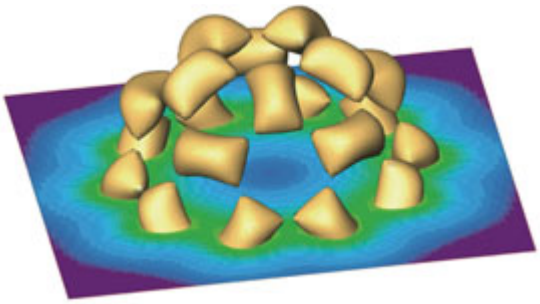

*Fig. 2: Momentum space representation of ELI-D for the $C_{60}$ molecule.*

**Choice of Pairs**

The space partitioning can be performed by fixing the pair density integral. However, there are different possibilities for this. The electron pair density can be split into contributions from the same-spin and opposite-spin electron pairs, respectively. As there is no Fermi-hole for the opposite-spin electrons, there will be different formulas for the pair density integrals and thus for ELI as well (due to the Taylor expansion). Even more, the calculation of the electron localizability indicator for the opposite-spin pairs is reasonable only at correlated level [7, 8]. In this case the space partitioning is based on the charge resulting in the form termed ELI-q.

For the same-spin form of ELI-D one must face the fact that in case of a spin-polarized calculation two ELI-D distributions, one for each spin, need to be analyzed. Such two distributions can be very different, especially when the majority-spin occupies antibonding orbitals, like for the spin-triplet $O_2$ molecule, cf. the diagrams (a) and (b) in Fig. 3.

Here, another decomposition of the 2-matrix can be utilized which is invariant with respect to the spin rotation and yields the 2-matrix as sum of two parts – the symmetric and the antisymmetric one. The corresponding electron densities and pair densities describe electrons coupled to a singlet and triplet, respectively. Following the restricted populations approach the above densities can be used for the ELI definition.

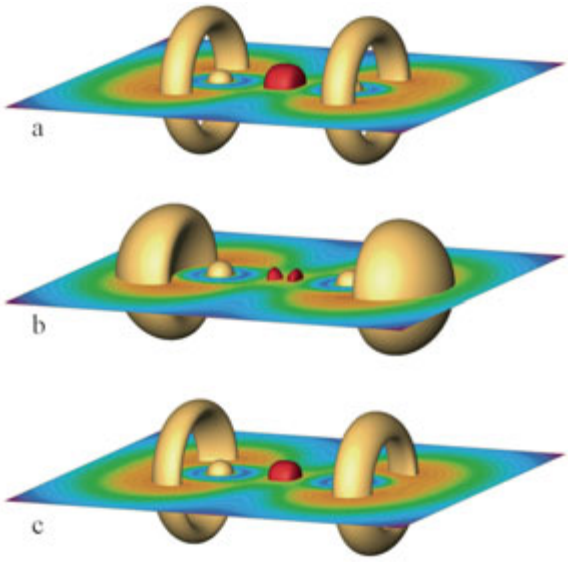


*Fig. 3: ELI-D for the $O_2$ molecule. (a) majority spin; (b) minority spin; (c) triplet-coupled electrons. Red ELI-D isosurfaces display the single-attractor and the split-attractor scenario, respectively.*

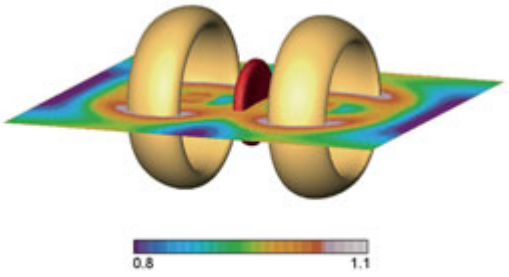


*Fig. 4: ELI-q for the $O_2$ molecule: singlet-coupled electrons. The red ELI-q isosurface displays the single-attractor scenario.*

As the density of the triplet-coupled electron pairs involves both αα and ββ same-spin pairs (and opposite-spin pairs as well), the corresponding ELI-D, cf. the diagram (c) in Fig. 3, results in a single distribution for the spin-polarized wavefunction [9].

The density of the singlet-coupled electrons involves only the opposite-spin electron pairs. To match the chemical expectation with respect to the chosen bonding descriptors (regions of high ELI values) the charge-restricted partitioning is chosen resulting in ELI-q. The ELI-q bonding descriptors for the singlet-coupled electrons emerge only at correlated level as shown in Fig. 4 for the $O_2$ molecule. Low ELI-q values are associated with regions where the electrons coupled to a singlet tend to avoid each other. The ELI-q values are connected with the tendency of the (fixed) electron population to couple to a singlet pair.

**Charge Decomposition of ELI-D**

The electron localizability indicator was defined to be proportional to a discrete charge distribution. For such a distribution the charge within each μ-cell can be given as the product of the electron density at the μ-cell center and the volume of the μ-cell (sufficiently small, with size controlled by the restriction). The discrete charge values can be formally decomposed into contributions, for instance from orbitals or orbital groups within a chosen energy range, or a region in *k*-space in case of a solid state calculation.

Actually, each ELI-D value can be seen as a product of the electron density and the so called pair-volume function (proportional to the volume of a fixed amount of electron pairs around given position). The orbital decomposition of ELI-D allows to analyze the contribution of particular orbitals to the electron localizability [10]. The distribution based on a chosen set of orbitals is abbreviated pELI-D ("p" for partial).

For instance, the $N_2$ molecule exhibits a single ELI-D bond attractor between the atoms. Why does the separation into two bond descriptors, representing the σ and π bonds, not occur? This can be seen from the pELI-D diagrams in Fig. 5. Inspection of

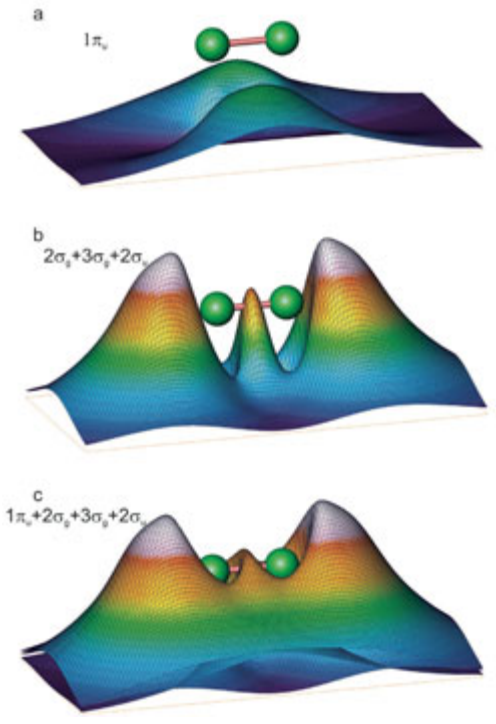


*Fig. 5: pELI-D for the $N_2$ molecule. (a) π orbital; (b) σ orbitals; (c) π and σ orbitals*

the diagram (a) shows, that the π contributions do form a ring attractor around the bond midpoint, whereas the sum of the σ contributions results in a point attractor. In the sum of all orbitals contributions the π part is not pronounced enough to give rise to a separate (total) ELI-D attractor.

High pELI-D contributions to the total value are achieved especially by localized orbitals. The diagram (a) in Fig. 6 depicts the pELI-D contributions of the Boys localized orbitals in the position space (e.g., the green isosurface is due to the π bonds). The correspondence of the pELI-D contributions to the distinct bonding features is clearly highlighted. This can be further utilized to find the correct correspondence between the ELI-D pattern in the real space and momentum space. Now, in the diagram (b) of Fig. 6 it is easy to recognize to which descriptor in the real space the momentum space regions corresponds to. It should be noted that the π bonds are localized above the $p_xp_y$ plane, i.e., located in region of momenta directed perpendicular to the molecular plane.

The evaluation of pELI-D was also utilized in the analysis of solid state density matrices. In this case the contributions of bands from separate energy ranges (DOS regions) are used [11,16].

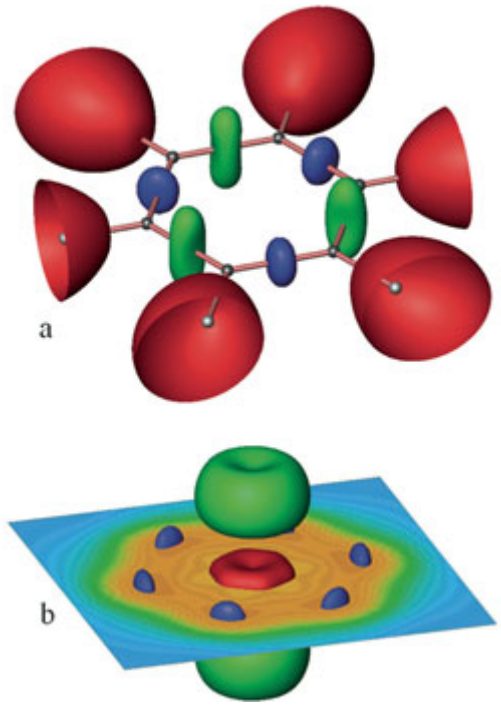


*Fig. 6: pELI-D for the $C_6H_6$ molecule. (a) localized orbital contributions in real space; (b) momentum space image. The colors of the pELI-D isosurface denote corresponding contributions of position and momentum space.*

**Direct Space Decomposition of ELI-D**

The ELI-D can be formally written as the product of the electron density and the pair-volume function. The topology of the distribution can be rationalized with the signature of the corresponding Laplacian. The occurrence of a maximum implies the existence of three negative principal curvatures of the analyzed function at the given position. The Laplacian of the ELI-D can formally be expressed as a sum involving the Laplacian of both the electron density and the pair-volume function as well as an additional mixed gradient term. With this procedure it is possible to rationalize the evident similarity between the topology of ELI-D and the topology of the electron density Laplacian [12]. However, even if the atomic shells are not resolved by the electron density Laplacian, like in case of transition metal atoms, ELI-D still shows the atomic shell structure due to the influence of the (always negative) mixed gradient term.

In case of the $F_2$ molecule there is a double maximum of ELI-D along the internuclear line [10], cf. Fig. 7. The topology of the electron density as well as the pair-volume function is the one expected for

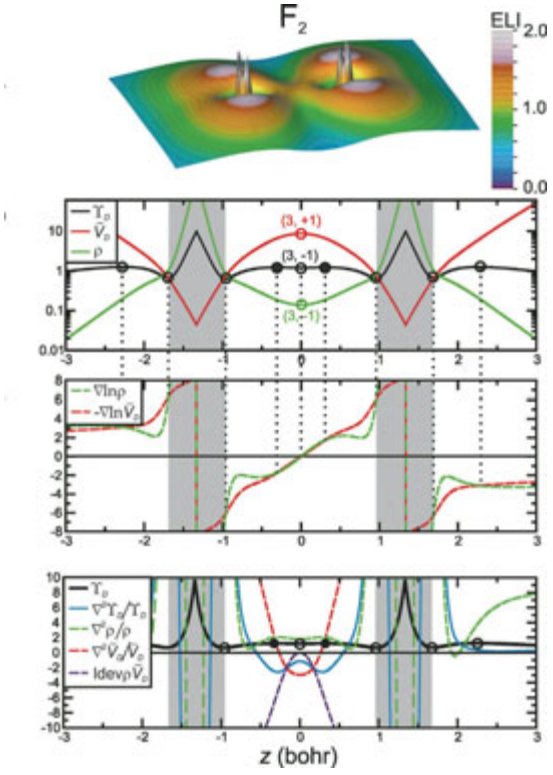


*Fig. 7: Direct space decomposition for the $F_2$ molecule. (a) ELI-D; (b) components along the internuclear line; (c) gradient terms; (d) relative Laplacian terms.*

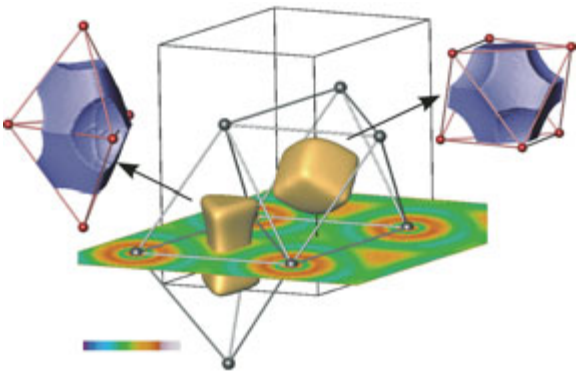

*Fig. 8: ELI-D for hexagonal Sc: isosurfaces and basins.*

a homonuclear dimer (bond critical point for the density and a ring critical point for the pair-volume function). The double-wave structure of the $\nabla \ln \rho$ curve, cf. the diagram (c) in Fig. 8, gives rise to the three critical points in the internuclear region, i.e., the double-maximum of ELI-D occurs. Remarkably, the relative Laplacian of the pair-volume function, see the diagram (d), is negative at the bond midpoint and displays a shape typical for a single bond. It is noteworthy that the density Laplacian is positive at the bond midpoint, even for a MRCI calculation. The negative Laplacian of ELI-D at the bond midpoint appears solely by the dominance of the negative relative Laplacian of the pair-volume function [12].

**Bond Descriptors**

Since ELI-D resolves the atomic shell structure up to Xe not only qualitatively, but also with electron populations (connected with the shells) that are close to the desired numbers from the Aufbau principle, there remains a conveniently defined valence region. In chemical systems, the complete valence region is further partitioned into parts (basins) which again have locations and electronic populations supporting chemical concepts.

An important topic is the analysis of metal–metal bonding situations. In a solid the variety of constellations of ELI-D localization domains and basins can be very high even for relatively simple structures. This variety has been utilized to classify the hexagonal element structures into seven patterns, depending on the location of ELI-D basins [13]. Fig. 8 presents the irreducible localization domains and the corresponding ELI-D basins for the hexagonal Sc, classified as pattern II. It can be seen that for this type there is one attractor in the octahedral position whereas a second one shares two tetrahedral voids.

For the understanding of the complex bonding scenarios in intermetallic solids the study of prototype molecular systems is of great importance. As a matter of fact, molecular systems can be treated with higher quantum mechanical (e.g. explicitly correlated density matrices) and technical accuracy (basis sets), and the structural complexity can be strongly reduced. These studies serve to generate new ideas about metal–metal bonding situations, which in turn lead to the development of new tools for their analysis. Recently, in our cooperation with Prof. R. Kempe (University of Bayreuth) within the DFG "Schwerpunktprogramm 1166" we analyzed one of the very rare examples of a non-bridged transition metal–rare earth metal bonding situation which occurs in homoleptic bimetallic complexes $Cp_2Re–RECp_2$ (with *RE* = Y, Yb; Cp = $C_5H_5$) [14]. The bonding turns out to be of a polar donor–acceptor type with the transition metal displaying a special type of lone pair. With the understanding of this type of interaction, the subsequent treatment of a more complex Os–La bonding situation as found in the intermetallic compound $La_7Os_4C_9$ was achieved [15]. The bimetallic donor–acceptor scenario is extended to a polymetallic one, where an Os species displays two lone pair type features, each of which is shared with up to five La neighbors (Fig. 9).

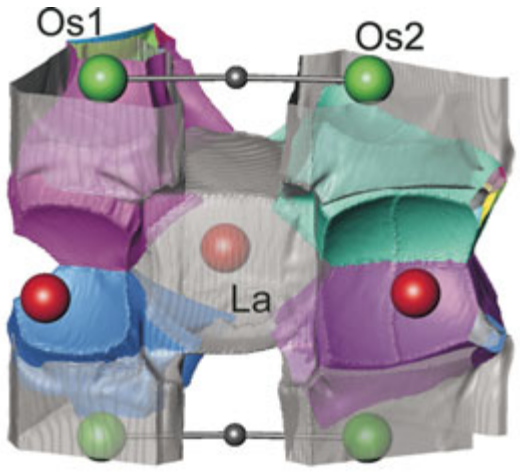


*Fig. 9: $La_7Os_4C_9$: Os–La bonding situation using ELI-D/QTAIM intersection. Translucent grey regions represent QTAIM Os and La atoms. Opaque regions display lone pair type ELI-D basins leaking out of the Os atomic regions (cut by a mirror plane) into the La atomic regions.*

Concerning homoatomic metal–metal bonding we recently analyzed an example of an "ultrashort" (within 1 pm the shortest metal–metal distance in a stable molecule at all) Cr–Cr bond of 175 pm occurring in an amidopyridinato-complex [16]. The chemical bonding description for this type of compounds which are claimed to display metal–metal 5-fold bonding (one σ-, two π-, and two δ-type bonds) represents a challenge, both for electronic structure methods for generating the wavefunction, and for chemical bonding descriptors. Our results, based on DFT calculations, yield signatures for weak δ-type bonding and a bond order (calculated from the delocalization index [2], mentioned in the "Introduction", between the QTAIM Cr atoms) of 4.2 [16]. The bonding scenario is characterized not only by electron localizability attractors in the valence region (Fig. 11), but also by sizable Cr($3^{rd}$ shell)–Cr($3^{rd}$ shell) delocalization index contributions of 2.4. This extreme case shows that a complete chemical bonding analysis in position space between transition elements needs to take into account those electrons from the penultimate shell, that are found to significantly delocalize into the valence region. In the case of transition metal single bonds much smaller values are calculated, e.g., a delocalization index value of 0.29 between the QTAIM Mn atoms in $Mn_2(CO)_{10}$ [17].

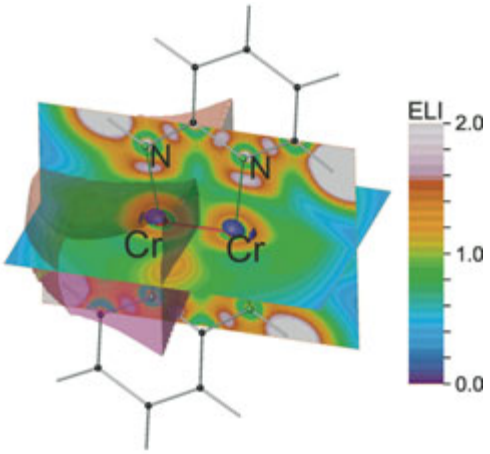


*Fig. 10: RCr–CrR with (R = $C_5NH_4NH$): ELI-D slices and blue 1.44-localization domain displaying penultimate shell structuring; translucent red surface shows Cr QTAIM basin.*

## Conclusion

With the use of ω-restricted space-partitioning various electron localizability measures have now been introduced which are all based on a general many-body time-dependent pair density. The physical transparency of these ELI variants gives rise to the development of analysis tools for a deeper understanding of the underlying mechanisms for the generation of distinct topological ELI features, that are specific for certain bonding scenarios. Together with the core part of QTAIM theory, pioneered by R. F. W. Bader and further developed by a small number of groups worldwide, they provide a powerful framework for the analysis of chemical bonding in physical space, i.e., position and momentum space.

## References

[1] *R. F. W. Bader,* in Atoms in Molecules – A Quantum Theory (Claredon Press, Oxford, 1995).
[2] *X. Fradera, M. A. Austen, and R. F. W. Bader,* J. Phys. Chem. A **103** (1999) 304.
[3] *M. Kohout,* Int. J. Quantum. Chem. **97** (2004) 651.
[4] *R. F. W. Bader, M. E. Stephens,* Chem. Phys. Lett. **26** (1974) 445.
[5] *M. Kohout, F. R. Wagner, and Yu. Grin,* Theor. Chem. Acc. **112** (2004) 453.
[6] *M. Kohout,* Faraday Discuss. **135** (2007) 43.
[7] *M. Kohout, F. R. Wagner, and Yu. Grin,* Theor. Chem. Acc. **113 (**2005) 287.
[8] *V. Bezugly, P. Wielgus, F. R. Wagner, M. Kohout, and Yu. Grin,* J. Comput. Chem. **29** (2008) 1198.
[9] *M. Kohout, F. R. Wagner, and Yu. Grin,* Theor. Chem. Acc. **119** (2008) 413.
[10] *F. R. Wagner, V. Bezugly, M. Kohout, and Yu. Grin,* Chem. Eur. J. **13** (2007) 5724.
[11] cf. "Concerning Carbo Compounds: On the Nature of $C_2$ Units"
[12] *F. R. Wagner, M. Kohout, and Yu. Grin,* J. Phys. Chem. A **112** (2008) 9814.
[13] *A. I. Baranov and M. Kohout,* J. Comp. Chem. **29** (2008) 2161.
[14] *M. V. Butovskii, O. L. Tok, F. R. Wagner, and R. Kempe,* Angew. Chem. Int. Ed. **47** (2008) 6469.
[15] *E. Dashjav, Y. Prots, G. Kreiner, W. Schnelle, F. R. Wagner, and R. Kniep,* J. Solid State Chem. **181** (2008) 3121.
[16] *A. Noor, F. R. Wagner, and R. Kempe,* Angew. Chem. Int. Ed. **47** (2008) 7246.
[17] *C. Gatti, D. Lasi*, Faraday Discuss. **135** (2007) 55.